Article

Structural and Dynamical Basis of Broad Substrate Specificity, Catalytic Mechanism, and Inhibition of Cytochrome P450 3A4

Hwangseo Park, Sangyoub Lee, and Junghun Suh

J. Am. Chem. Soc., **2005**, 127 (39), 13634-13642• DOI: 10.1021/ja053809q • Publication Date (Web): 07 September 2005

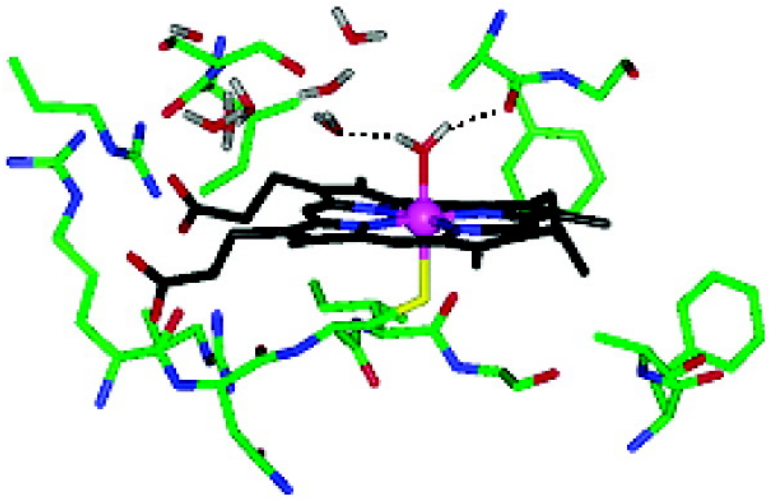

J|A|C|S
ARTICLES
Published on Web 09/07/2005

Structural and Dynamical Basis of Broad Substrate Specificity, Catalytic Mechanism, and Inhibition of Cytochrome P450 3A4

Hwangseo Park,* Sangyoub Lee,* and Junghun Suh

Contribution from the Department of Chemistry, Seoul National University, Seoul 151-747, South Korea

Received June 10, 2005; E-mail: hwangseo@snu.ac.kr; sangyoub@snu.ac.kr

Abstract: Cytochrome P450 (CYP) 3A4 is responsible for the oxidative degradation of more than 50% of clinically used drugs. By means of molecular dynamics simulations with the newly developed force field parameters for the heme−thiolate group and its dioxygen adduct, we examine the differences in structural and dynamic properties between CYP3A4 in the resting form and its complexes with the substrate progesterone and the inhibitor metyrapone. The results indicate that the broad substrate specificity of CYP3A4 stems from the malleability of a loop (residues 211−218) that resides in the vicinity of the channel connecting the active site and bulk solvent. However, the high-amplitude motion of the flexible loop is found to be damped out upon binding of the inhibitor or the substrate in the active site. In the resting form of CYP3A4, a structural water molecule is bound to the sixth coordination position of the heme iron, stabilizing the octahedral coordination geometry. In addition to the direct coordination of metyrapone to the heme iron, the hydrogen bond interaction between the inhibitor carbonyl group and the side chain of Ser119 also contributes significantly to stabilizing the CYP3A4−metyrapone complex. On the other hand, progesterone is stabilized in the active site by the formation of two hydrogen bonds with Ser119 and Arg106, as well as by the van der Waals interactions with the heme and hydrophobic residues. The structural and dynamic features of the CYP3A4−progesterone complex indicate that the oxidative degradation of progesterone occurs through hydroxylation at the C16 position by the reactive oxygen coordinated to the heme iron.

Introduction

Cytochromes P450 (CYPs) are a class of heme−thiolate enzymes and represent the major catalysts for the oxidative degradation of a wide range of endogenous compounds, drugs, and other xenobiotics, such as pollutants and environmental chemicals. The microsomal membrane-associated CYP isoforms include CYP3A4, CYP2D6, CYP2C9, CYP2C19, CYP2E1, and CYP1A2, which account for the oxidation of approximately 90% of drugs currently on the market. Among the various isoforms, CYP3A4 is the most abundant one in human liver microsomes, constituting 30% of the total population for CYPs. CYP3A4 is also known to have a broad substrate specificity and metabolize more than 50% of clinically used drugs.[1,2] Because both low clearance and oral bioavailability of a drug candidate depend on its ability to withstand the degradation by metabolizing enzymes, the stability toward CYP3A4 is one of the most important properties that have to be measured and estimated in the early stage of drug discovery.[3,4]

CYP3A4 shows atypical kinetic behavior[5,6] toward a number of substrates, including amitriptyline,[7] caffeine,[8] carbamazepine,[9] progesterone,[10] and diazepam.[11] These substrates yield a sigmoidal v versus S plot, indicative of positive homotropic cooperativity. In contrast, effectors such as α-naphthoflavone[10,12] and testosterone[9] cause the stimulation of CYP3A4 toward some substrates, which is referred to as heterotropic cooperativity.[13−15] In the absence of X-ray crystal structure, homology modeling and site-directed mutagenesis studies were carried out to investigate the structural features relevant to the broad substrate specificity of CYP3A4.[16−20] It was suggested that the cooper-

(1) Guengerich, F. P. *Chem. Res. Toxicol.* **2001**, *14*, 611−650.
(2) Wrighton, S. A.; Schuetz, E. G.; Thummel, K. E.; Shen, D. D.; Korzekwa, K. R.; Watkins, P. B. *Drug Metab. Rev.* **2000**, *32*, 339−361.
(3) Boobis, A.; Gundert-Remy, U.; Kremers, P.; Macheras, P.; Pelkonen, O. *Eur. J. Pharm. Sci.* **2002**, *17*, 183−193.
(4) Kumar, G. N.; Surapaneni, S. *Med. Res. Rev.* **2001**, *21*, 397−411.
(5) Guengerich, F. P. *Annu. Rev. Pharmacol. Toxicol.* **1999**, *39*, 1−17.
(6) Hutzler, J. M.; Tracy, T. S. *Drug Metab. Dispos.* **2002**, *30*, 355−362.
(7) Ueng, Y. F.; Kuwabara, T.; Chun, Y. J.; Guengerich, F. P. *Biochemistry* **1997**, *36*, 370−381.
(8) Grant, D. M.; Campbell, M. E.; Tang, B. K.; Kalow, W. *Biochem. Pharmacol.* **1987**, *36*, 1251−1260.
(9) Kerr, B. M.; Thummel, K. E.; Wurden, C. J.; Klein, S. M.; Kroetz, D. L.; Gonzalez, F. J.; Levy, R. H. *Biochem. Pharmacol.* **1994**, *47*, 1969−1979.
(10) Schwab, G. E.; Raucy, J. L.; Johnson, E. F. *Mol. Pharmacol.* **1988**, *33*, 493−499.
(11) Shou, M.; Mei, Q.; Ettore, M. W.; Dai, R.; Baillie, T. A.; Rushmore, T. H. *Biochem. J.* **1999**, *340*, 845−853.
(12) Harlow, G. R.; Halpert, J. R. *Proc. Natl. Acad. Sci. U.S.A.* **1998**, *95*, 6636−6641.
(13) Lasker, J. M.; Huang, M. T.; Conney, A. H. *Science* **1982**, *216*, 1419−1421.
(14) Tang, W.; Stearns, R. A.; Wang, R. W.; Chiu, S.-H. L.; Baillie, T. A. *Chem. Res. Toxicol.* **1999**, *12*, 192−199.
(15) Tang, W.; Stearns, R. A.; Kwei, G. L.; Iliff, S. A.; Miller, R. R.; Egan, M. A.; Yu, N. X.; Dean, D. C.; Kumar, S.; Shou, M.; Lin, J. H.; Baillie, T. A. *J. Pharmacol. Exp. Ther.* **1999**, *291*, 1068−1074.
(16) Kuhn, B.; Jacobsen, W.; Christians, U.; Benet, L. Z.; Kollman, P. A. *J. Med. Chem.* **2001**, *44*, 2027−2034.
(17) Szklarz, G. D.; Halpert, J. R. *J. Comput.-Aided Mol. Des.* **1997**, *11*, 265−272.
(18) Domanski, T. L.; Liu, J.; Harlow, G. R.; Halpert, J. R. *Arch. Biochem. Biophys.* **1998**, *350*, 223−232.

10.1021/ja053809q CCC: $30.25

ativity in the reaction mechanism of CYP3A4 could be attributed either to the ability of the extensive active site to accommodate more than one substrate molecule simultaneously or to the existence of functionally distinct conformers. Along with the mechanistic studies, a number of structurally diverse inhibitors of CYP3A4 have been discovered.[21−27] Now it is common practice in drug discovery to screen chemicals that possess inhibitory activity against CYP3A4-mediated metabolism.

Recently, Williams et al. reported X-ray crystal structures of CYP3A4 with low-spin ferric heme in the resting form and its two complexes with the inhibitor metyrapone and the substrate progesterone.[28] CYP3A4 reveals a fold similar to that of the CYP superfamily, which has the heme group in the active site and comprises a small β-strand N-terminal and a larger α-helical C-terminal domains.[29−31] The heme iron is ligated by the side chain thiolate group of the conserved cystein residue (Cys442). However, the structure of CYP3A4 differs from the other CYPs in that it has a hydrophobic region (residues 36−50) around a loop in the N-terminal domain. Another unexpected structural feature of CYP3A4 is the short helix (F helix) consisting of residues 203−210. CYP3A4 has a small active site, which undergoes little conformational change in the presence of the inhibitor or the substrate. The pyridinyl ring of the inhibitor metyrapone interacts with heme through direct coordination to the central heme iron. On the other hand, the substrate progesterone is bound to a peripheral site near the Phe cluster that lies above the active site with the aromatic side chains stacking against each other to form a prominent hydrophobic core. On the basis of this finding, Williams et al. proposed that such a peripheral binding site may be involved in the recognition of effector and substrate molecules.[28] However, it remains unclear if the substrate can be docked into the active site in an orientation consistent with the oxidative degradation.

Complementary to a large amount of experimental work, several theoretical studies on CYPs have also been reported to address the catalytic mechanism and substrate specificity,[32−36] to predict binding affinities of various ligands,[37−39] and to estimate the stabilities of drug-like molecules against CYP3A4-mediated metabolism.[40−42] In the present study, we examine the dynamic properties of CYP3A4 in the resting form as compared to those of its complexes with the inhibitor metyrapone and the substrate progesterone (Figure 1) by means of solution-phase molecular dynamics (MD) simulations. We focus our interest on clarifying the roles of solvent dynamics and the loop structures near the active site in the binding of the ligands and in stabilizing the coordination structure of the heme iron. On the basis of docking experiments and MD simulations, we investigate the possibility of binding progesterone in the active site of CYP3A4 and the structural features of the CYP3A4−progesterone complex pertinent to the catalytic mechanism for oxidative degradation of the substrate. Newly developed force field parameters for the heme−thiolate group and its dioxygen adduct are used in the simulations due to the lack of them in the standard force field database. The detailed structural and dynamic properties found in this comparative MD study of CYP3A4 are expected to provide insight into ligand binding, catalytic mechanisms, and estimating the metabolic stability for a compound of a drug candidate.

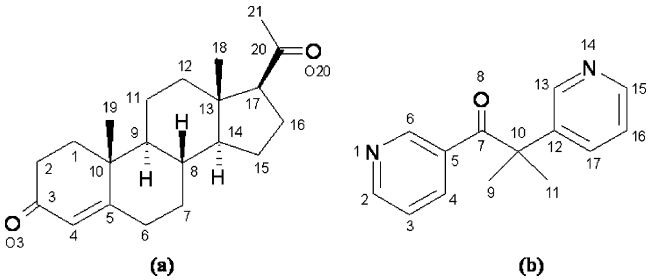

Figure 1. Molecular structures and numbering of (a) the substrate progesterone and (b) the inhibitor metyrapone.

Computational Methods

Force Field Design for the Heme−Thiolate Group and its Dioxygen Adduct. The bonded approach proposed by Hoops et al.[43] and Ryde[44] was adopted to introduce explicit bonds between the central heme iron and its ligand atoms. This choice was based on the earlier computational finding that other nonbonded approaches had been sensitive to the electrostatic model used, leading to an undesirable coordination geometry at metal centers.[45] To derive the associated force field parameters that are unavailable in the standard force field database, we followed the procedure suggested by Fox and Kollman[46] to be consistent with the standard AMBER force field.[47] The equilibrium bond lengths and bond angles involving the heme iron were taken from the optimized structures of the heme−thiolate group and its dioxygen adduct. These geometry optimizations were performed at the B3LYP/

(19) Harlow, G. R.; Halpert, J. R. *J. Biol. Chem.* **1997**, *272*, 5396−5402.
(20) He, Y. A.; He, Y. Q.; Szklarz, G. D.; Halpert, J. R. *Biochemistry* **1997**, *36*, 8831−8839.
(21) Usia, T.; Iwata, H.; Hiratsuka, A.; Watabe, T.; Kadota, S.; Tezuka, Y. *J. Nat. Prod.* **2004**, *67*, 1079−1083.
(22) Alvarez-Diez, T. M.; Zheng, J. *Chem. Res. Toxicol.* **2004**, *17*, 150−157.
(23) Wu, Y.-J. et al. *J. Med. Chem.* **2003**, *46*, 3778−3781.
(24) Tsukamoto, S.; Tomise, K.; Miyakawa, K.; Cha, B.-C.; Abe, T.; Hamada, T.; Hirota, H.; Ohta, T. *Bioorg. Med. Chem.* **2002**, *10*, 2981−2985.
(25) Ohta, T.; Nagahashi, M.; Hosoi, S.; Tsukamoto, S. *Bioorg. Med. Chem.* **2002**, *10*, 969−973.
(26) Ohta, T.; Maruyama, T.; Nagahashi, M.; Miyamoto, Y.; Hosoi, S.; Kiuchi, F.; Yamazoe, Y.; Tsukamoto, S. *Tetrahedron* **2002**, *58*, 6631−6635.
(27) Tsukamoto, S.; Cha, B.-C.; Ohta, T. *Tetrahedron* **2002**, *58*, 1667−1671.
(28) Williams, P. A.; Cosme, J.; Vinkovic, D. M.; Ward, A.; Angove, H. C.; Day, P. J.; Vonrhein, C.; Tickle, I. J.; Jhoti, H. *Science* **2004**, *305*, 683−686.
(29) Williams, P. A.; Cosme, J.; Ward, A.; Angove, H. C.; Vinkovic, D. M.; Jhoti, H. *Nature* **2003**, *424*, 464−468.
(30) Sevrioukova, I. F.; Li, H.; Zhang, H.; Peterson, J. A.; Poulos, T. L. *Proc. Natl. Acad. Sci. U.S.A.* **1999**, *96*, 1863−1868.
(31) Cupp-Vickery, J. R.; Poulos, T. L. *Nat. Struct. Biol.* **1995**, *2*, 144−153.
(32) Denisov, I. G.; Makris, T. M.; Sligar, S. G.; Schlichting, I. *Chem. Rev.* **2005**, *105*, 2253−2278.
(33) Shaik, S.; Kumar, D.; de Visser, S. P.; Altun, A.; Thiel, W. *Chem. Rev.* **2005**, *105*, 2279−2328.
(34) Wade, R. C.; Winn, P. J.; Schlichting, I.; Sudarko, *J. Inorg. Biochem.* **2004**, *98*, 1175−1182.
(35) Winn, P. J.; Lüdemann, S. K.; Gauges, R.; Lounnas, V.; Wade, R. C. *Proc. Natl. Acad. Sci. U.S.A.* **2002**, *99*, 5361−5366.
(36) De Voss, J. J.; Sibbesen, O.; Zhang, Z.; Ortiz de Montellano, P. R. *J. Am. Chem. Soc.* **1997**, *119*, 5489−5498.
(37) Lewis, D. F. V.; Jacobs, M. N.; Dickins, M. *Drug Discovery Today* **2004**, *9*, 530−537.
(38) Susnow, R. G.; Dixon, S. L. *J. Chem. Inf. Comput. Sci.* **2003**, *43*, 1308−1315.
(39) Harris, D. L.; Park, J.-Y.; Gruenke, L.; Waskell, L. *Proteins* **2004**, *55*, 895−914.
(40)) Crivori, P.; Zamora, I.; Speed, B.; Orrenius, C.; Poggesi, I. *J. Comput.-Aided Mol. Des.* **2004**, *18*, 155−166.
(41) Singh, S. B.; Shen, L. Q.; Walker, M. J.; Sheridan, R. P. *J. Med. Chem.* **2003**, *46*, 1330−1336.
(42) Kemp, C. A.; Flanagan, J. U.; van Eldik, A. J.; Marechal, J.-D.; Wolf, C. R.; Roberts, G. C. K.; Paine, M. J. I.; Sutcliffe, M. J. *J. Med. Chem.* **2004**, *47*, 5340−5346.
(43) Hoops, S. C.; Anderson, K. W.; Merz, K. M., Jr. *J. Am. Chem. Soc.* **1991**, *113*, 8262−8270.
(44) Ryde, U. *Proteins* **1995**, *21*, 40−56.
(45) Stote, R. H.; Karplus, M. *Proteins* **1995**, *23*, 12−31.
(46) Fox, T.; Kollman, P. A. *J. Phys. Chem B* **1998**, *102*, 8070−8079.
(47) Cornell, W. D.; Cieplak, P.; Bayly, C. I.; Gould, I. R.; Merz, K. M., Jr.; Ferguson, D. M.; Spellmeyer, D. C.; Fox, T.; Caldwell, J. W.; Kollman, P. A. *J. Am. Chem. Soc.* **1995**, *117*, 5179−5197.

6-31G* level of theory with the JAGUAR program[48] on the model system in which the methyl thiolate ion, CH_3S^-, was used to represent Cys442 coordinated to the heme iron. For the force constant parameters involving the heme iron, we used the values in Giammona's earlier work.[49] Using energy-minimized structures, atomic partial charges were derived at the RHF/6-31G* level of theory with the RESP method[50,51] to be consistent with the standard AMBER force field. All of the torsions involving the metal−ligand bonds were set to zero as in Giammona's work.[49] Other missing force field parameters for heme were estimated from similar chemical species in the AMBER force field database. We derived the potential parameters for metyrapone and progesterone by following the same procedure as those for the heme−thiolate group, which involves geometry optimization and charge fitting with the RESP method.

Docking Simulation. The binding mode of progesterone in the active site of CYP3A4 was estimated by docking simulation with the AutoDock 3.0.5 program. It combines a rapid energy evaluation through the precalculated grids of affinity potentials with the Lamarckian genetic algorithm to find suitable binding positions for a ligand on a protein receptor.[52] Although the protein structure has to be fixed, the program allows torsional flexibility of a ligand. The coordinates of the protein atoms were taken from the X-ray crystal structures (PDB entry: 1W0E, 1W0F, and 1W0G) reported by Williams et al.[28] In this docking simulation, we used the empirical scoring function that has the following form:

$$\Delta G^{\mathrm{aq}}_{\mathrm{bind}} = W_{\mathrm{vdW}}\sum_i\sum_j\left(\frac{A_{ij}}{r_{ij}^{12}} - \frac{B_{ij}}{r_{ij}^{6}}\right) + W_{\mathrm{hbond}}\sum_i\sum_j E(t)\left(\frac{C_{ij}}{r_{ij}^{12}} - \frac{D_{ij}}{r_{ij}^{10}}\right) + W_{\mathrm{elec}}\sum_i\sum_j\frac{q_iq_j}{\epsilon r_{ij}} + W_{\mathrm{tor}}N_{\mathrm{tor}} + W_{\mathrm{sol}}\sum_i\sum_j(S_iV_j + S_jV_i)\exp(-r_{ij}^2/2\sigma^2) \quad (1)$$

where W_{vdW}, W_{hbond}, W_{elec}, W_{tor}, and W_{sol} are weighting factors of van der Waals, hydrogen bond, electrostatic interactions, torsional term, and desolvation energy of inhibitors, respectively. The hydrogen bond term has an additional weighting factor, $E(t)$, representing the angle-dependent directionality. A sigmoidal distance-dependent dielectric function proposed by Mehler et al.[53] was used in computing the interatomic electrostatic interactions between CYP3A4 and its ligands. In the desolvation term, S_i and V_i are the solvation parameter and the fragmental volume of atom i,[54] respectively. Of the conformations obtained from 20 independent docking runs, those clustered together have similar binding modes, differing by less than 1.0 Å in positional root-mean-square deviation. The most stable configuration of the protein−ligand complex was then selected for further analysis.

MD Simulations. MD simulations of CYP3A4 and its complexes with metyrapone and progesterone were carried out using the SANDER module of AMBER 7[55] with the newly developed force field parameters for the heme−thiolate group in addition to those reported by Cornell et al.[47] As starting structures, we used X-ray structures for CYP3A4 in the resting form, the CYP3A4−metyrapone complex, and the CYP3A4−progesterone complex in which the substrate resides in the peripheral binding site. For the CYP3A4−progesterone complex, in which the substrate is bound in the active site, the most stable complex found in the docking simulation was used as an input structure for subsequent MD simulations. The coordinates of all missing residues in the original X-ray structures were constructed from homology modeling using the coordinates of P450BM3 as a structural template. Although CYP3A4 is a membrane-bound protein, it is known to also be active in various aqueous solutions, and only water molecules were found on the surface of CYP3A4 in the crystal structures.[28] In addition, CYP3A4 displays a sigmoidal substrate−velocity curve in membrane as in aqueous solutions,[56] indicating the similarity of the catalytic mechanisms in the two different environments. From these experimental findings, we believe that the dynamic properties of CYP3A4 obtained in solution would not be very different from those in microsomal membrane. Therefore, we selected water molecules as solvent in MD simulations using the TIP3P[57] model. The all-atom models for the unliganded and liganded CYP3A4 were then immersed in rectangular boxes containing about 20 000 TIP3P water molecules. The reasonableness of this solvation model will be supported by the fact that both the conformation of CYP3A4 and the motions of its ligands in the binding sites are maintained stable during the entire course of simulation. After 1000 cycles of energy minimization to remove the bad steric contacts, we equilibrated the systems beginning with 20 ps equilibration dynamics of the solvent molecules at 300 K. The next step involved the equilibration of the solute with a fixed configuration of the solvent molecules consecutively at 10, 50, 100, 150, 200, 250, and 300 K for 10 ps at each temperature. Then, the equilibration dynamics of the entire system was performed at 300 K for 100 ps. Following the equilibration procedure, 1.8 ns MD simulations were carried out with periodic boundary conditions in the NPT ensemble. The temperature and pressure were kept at 300 K and 1 atm using Berendsen temperature coupling[58] and isotropic molecule-based scaling, respectively. The SHAKE algorithm,[59] with a tolerance of 10^{-6}, was applied to fix all bond lengths involving a hydrogen atom. We used a time step of 1.5 fs and a nonbond interaction cutoff radius of 12 Å; the trajectory was sampled every 0.15 ps (100 step intervals).

Results and Discussion

Force Field Parametrization of the Heme−Thiolate Group. To extend the AMBER force field for modeling the heme−thiolate group in CYP3A4 and its dioxygen adduct, we used the standard procedure to derive the potential parameters for metalloproteins. The method involves geometry optimization of the two groups at the B3LYP/6-31G* level of theory. Here, we assumed low-spin (doublet) ferric and low-spin (singlet) ferrous heme iron for the heme−thiolate group and for its dioxygen adduct, respectively. These choices were based on the crystallization conditions for the X-ray structures of CYP3A4 in the resting form[28] and for the dioxygen adduct of P450cam[60] from which the input structures for the calculations were extracted. Figure 2 displays the two structures of local energy minima. In the absence of dioxygen, the heme iron reveals a distorted square pyramidal coordination with respect to four pyrrole moieties of the protoporphyrin IX ligand and the thiolate group of Cys442, which is consistent with its coordination pattern in the crystal structure. The dioxygen molecule is stabilized at the sixth coordination position of the heme iron,

(48) Ringnalda, M. N. *Jaguar*; Schroedinger Inc.: Portland, OR, 1997.
(49) Giammona, D. A. Ph.D. Thesis, University of California, Davis, 1984.
(50) Besler, B. H.; Merz, K. M., Jr.; Kollman, P. A. *J. Comput. Chem.* **1990**, *11*, 431−439.
(51) Bayly, C. A.; Cieplak, P.; Cornell, W. D.; Kollman, P. A. *J. Phys. Chem.* **1993**, *97*, 10269−10280.
(52) Morris, G. M.; Goodsell, D. S.; Halliday, R. S.; Huey, R.; Hart, W. E.; Belew, R. K.; Olson, A. J. *J. Comput. Chem.* **1998**, *19*, 1639−1662.
(53) Mehler, E. L.; Solmajer, T. *Protein Eng.* **1991**, *4*, 903−910.
(54) Stouten, P. F. W.; Frömmel, C.; Nakamura, H.; Sander, C. *Mol. Simul.* **1993**, *10*, 97−120.
(55) Case, D. A. et al. *AMBER 7*, University of California, San Francisco, 2002.
(56) Schrag, M. L.; Wienkers, L. C. *Drug Metab. Dispos.* **2000**, *28*, 1198−1201.
(57) Jorgensen, W. L.; Chandrasekhar, J.; Madura, J. D.; Impey, R. W.; Klein, M. L. *J. Chem. Phys.* **1983**, *79*, 926−935.
(58) Berendsen, H. C.; Postma, J. P. M.; van Gunsteren, W. F.; DiNola, A.; Haak, J. R. *J. Chem. Phys.* **1984**, *81*, 3684−3690.
(59) Ryckaert, J. P.; Ciccotti, G.; Berendsen, H. C. *J. Comput. Phys.* **1977**, *23*, 327−341.
(60) Schlichting, I.; Berendzen, J.; Chu, K.; Stock, A. M.; Maves, S. A.; Benson, D. E.; Sweet, R. M.; Ringe, D.; Petsko, G. A.; Sligar, S. G. *Science* **2000**, *287*, 1615−1622.

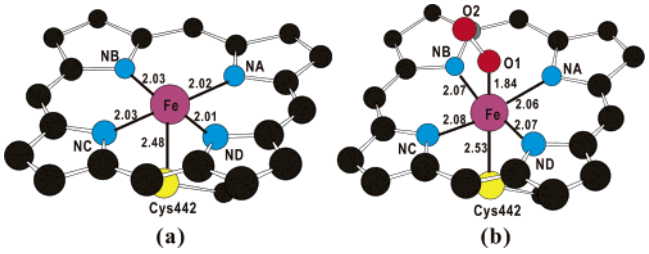

Figure 2. B3LYP/6-31G* optimized structures of (a) the heme−thiolate group and (b) its dioxygen adduct. The internuclear distances between the central heme iron and its ligand atoms are given in angstroms. All hydrogen atoms and side chain groups of heme are omitted for simplicity.

Table 1. Calculated RESP Charges (in e) of the Heme Iron and Its Ligand Atoms in the Heme−Thiolate Group and Its Dioxygen Adduct[a]

Heme–Thiolate		Dioxygen Adduct of Heme–Thiolate	
atoms	RESP charges	atoms	RESP charges
Fe	1.198 (3.000)	Fe	0.794 (2.000)
Heme NA	−0.283 (−0.414)	Heme NA	−0.322 (−0.414)
Heme NB	−0.285 (−0.409)	Heme NB	−0.326 (−0.409)
Heme NC	−0.279 (−0.412)	Heme NC	−0.322 (−0.412)
Heme ND	−0.282 (−0.411)	Heme ND	−0.319 (−0.411)
Cys442 SG	−0.311 (−0.736)	Cys442 SG	−0.397 (−0.736)
		O1	−0.131 (0.000)
		O2	−0.164 (0.000)

[a] Numbers in parentheses indicate the atomic charges before the formation of a metal complex.

as in the crystal structure, to form an octahedral coordination for the heme iron. Interatomic distances associated with the heme iron compare reasonably well with those in the crystal structures with a difference of 0.04 Å on average.

Table 1 lists the calculated RESP atomic charges of the central heme iron and its ligand atoms in the optimized structures of the heme−thiolate group and its dioxygen adduct. We note that the atomic charge of the heme iron decreases from +3.000 to +1.198 e in the heme−thiolate group, and from +2.000 to +0.794 e in its dioxygen adduct. On the other hand, the atomic charges of ligand atoms become less negative by 0.083−0.161 e for the nitrogen atoms of the protoporphyrin IX ligand, and by 0.339−0.448 e for the thiolate group as compared to those in the absence of the heme iron. These changes reflect the redistribution of charges between the heme iron and its ligand atoms upon formation of the metal complexes. It is noteworthy that the first (O1) and the second (O2) oxygen atoms of the dioxygen molecule bound to the heme iron have negative charges of −0.131 and −0.164 e, respectively, which is consistent with the earlier computational results reported by Scherlis et al.[61] This result indicates that a significant amount of electron density is transferred from the heme iron to the oxygen molecule, exemplifying the metal-to-π^* back-donation. We used these newly obtained atomic charges in MD simulations of unliganded and liganded CYP3A4 because it is well-attested that the "M^{n+}" model for a metal ion is inadequate for maintaining the actual coordination geometry observed in the active sites of metalloenzymes.[44,45]

Docking Simulations of Metyrapone and Progesterone. To estimate the accuracy of the AutoDock program in predicting the binding modes of the ligands to CYP3A4, we examined the reproducibility of the bound conformations in the X-ray crystal structures for metyrapone in the active site and for progesterone in the peripheral binding site. As shown in Table 2, the root-mean-square deviation (RMSD) between the bound conformation in the X-ray structure and the most stable conformation generated with AutoDock falls under 1.1 Å in both cases. These validation results indicate that the binding mode of progesterone in the CYP3A4 active site can be estimated from the docking simulation with AutoDock, and the resulting lowest-energy CYP3A4−progesterone complex may be a reasonable choice as a starting point for probing dynamic properties of the enzyme−substrate complex.

Table 2. Validation Results for AutoDock 3.0.5 in the Prediction of Binding Modes in the Two X-ray Structures of CYP3A4−Ligand Complexes, Together with the Binding Energies Calculated with Equation 1[a]

PDB code	RMSD of top score (Å)	binding energy (kcal/mol)
1W0F	0.73	−14.5
1W0G	1.09	−14.2

[a] 1W0F and 1W0G correspond to CYP3A4−progesterone and CYP3A4−metyrapone complexes, respectively.

Prior to the docking simulation of the substrate progesterone in the active site of CYP3A4, the dioxygen molecule was placed at the sixth coordination position of the heme iron according to the coordination structure in the dioxygen adduct of P450cam. The analysis of the binding mode and binding free energy for progesterone in the oxygen-bound CYP3A4 is believed to provide insight into the mechanistic features of its oxidative degradation in the active site of CYP3A4. Figure 3 shows the lowest-energy AutoDock conformation and binding free energy of progesterone in the dioxygen adduct of CYP3A4. It is seen that progesterone is docked in the active site with a binding free energy of −17.9 kcal/mol in the same conformation as in the peripheral binding site observed in the X-ray crystal structure. This binding free energy in the active site is predicted to be 3.4 kcal/mol lower than that in the peripheral binding site (Table 2). This difference indicates that the catalytic mechanism of CYP3A4 would involve the initial recognition of progesterone in the peripheral binding site and its movement to the active site, in which an extra stabilization can be attained. In the CYP3A4−progesterone complex with dioxygen, the 3-carbonyl oxygen (O3) of progesterone is directed to the backbone group of Arg106 while the 20-keto group points toward Ala305. The steroid ring of progesterone forms van der Waals contacts with the heme group as well as with the side chains of Arg105, Phe108, Ile120, Ile301, and Phe304.

However, it has been suggested that the oxygen molecule replaces a water ligand at the sixth coordination position of the heme iron after progesterone binds to the active site.[32] Therefore, we also carried out docking simulation of progesterone in the active site with a water molecule bound to the heme iron. The calculated binding energy is −17.5 kcal/mol, which is 0.4 kcal/mol less favorable than the result obtained with dioxygen in the active site. This seems to support the possibility of the ligand exchange at the heme iron upon substrate binding.

Dynamic Properties of Unliganded and Liganded CYP3A4. Shown in Figure 4 are time evolutions of the root-mean-square deviations from initial structures ($RMSD_{init}$) for all C_α atoms of CYP3A4 in comparison with those for all heavy atoms of the ligands. In both bound and unbound simulations, the

(61) Scherlis, D.; Estrin, D. A. *J. Am. Chem. Soc.* **2001**, *123*, 8436−8437.

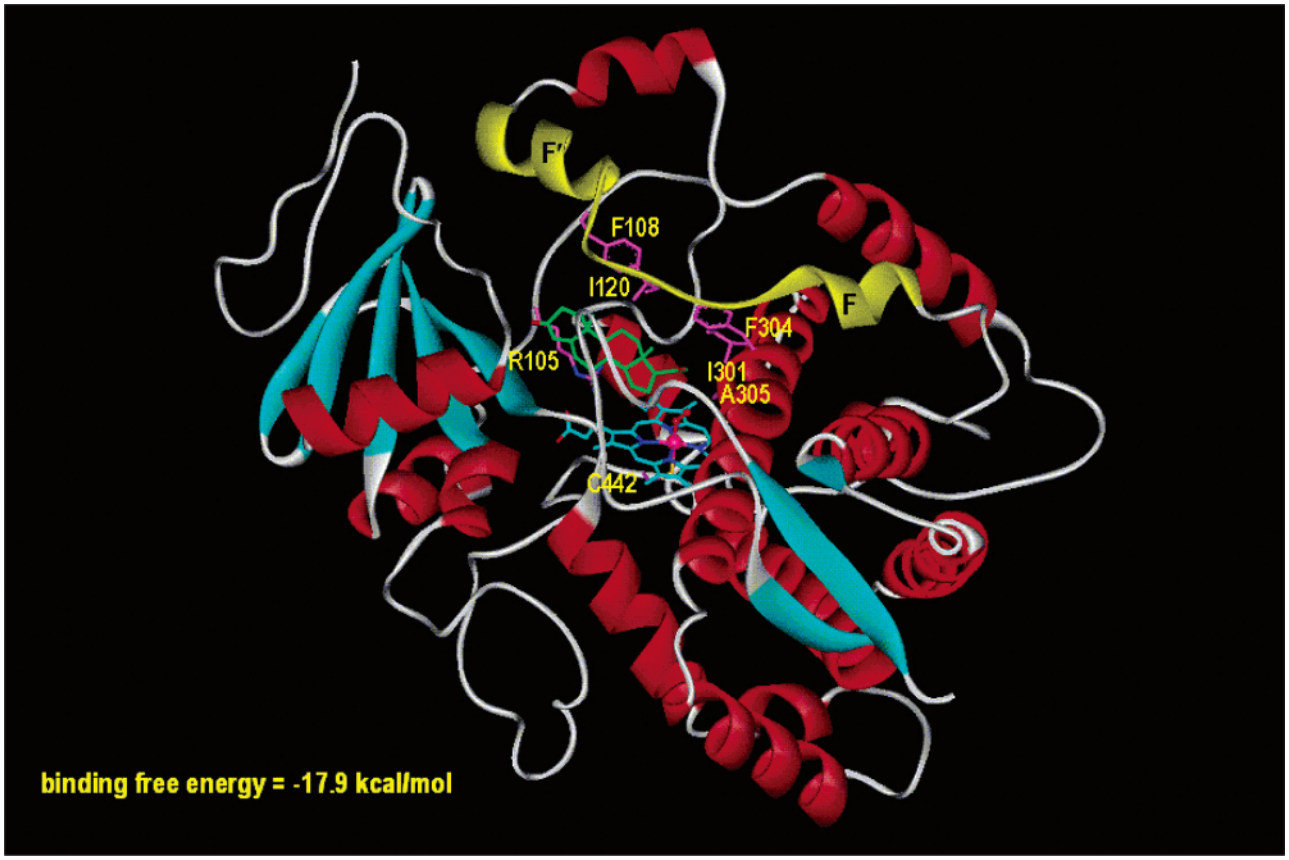

Figure 3. Binding mode of progesterone in the active site of CYP3A4. Carbon atoms of heme, progesterone, and active site residues are shown in cyan, green, and magenta, respectively. Indicated in yellow are F and F′ helices and the flexible loop (residues 211−218) connecting the two helices.

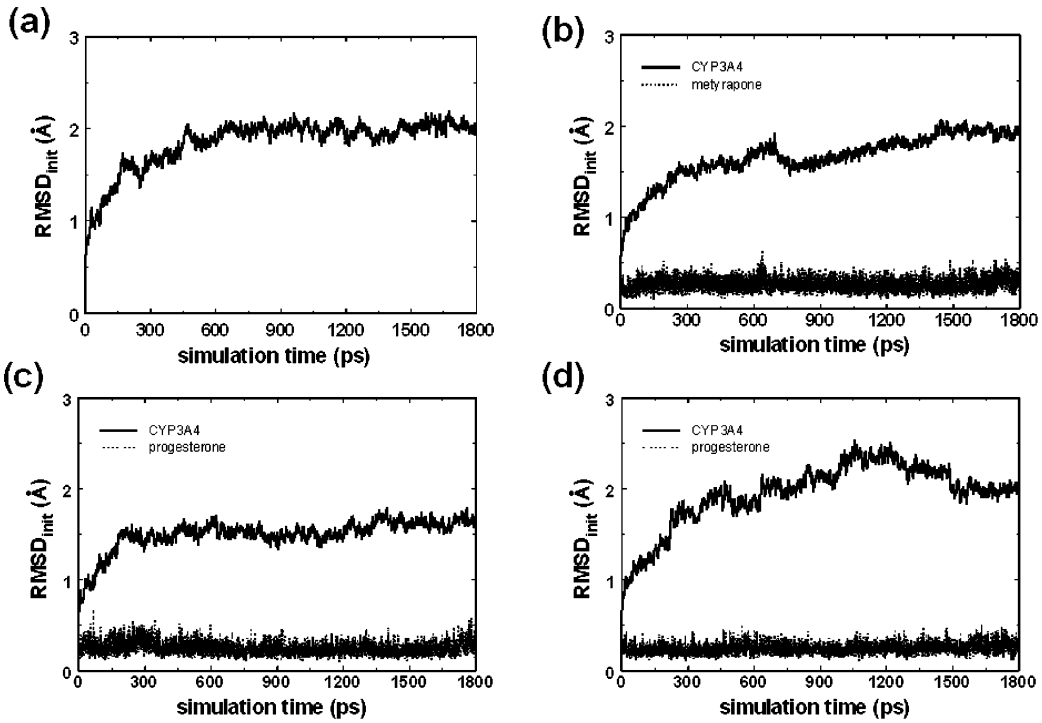

Figure 4. Time dependences of root-mean-square deviations from the initial structures ($RMSD_{init}$) for (a) CYP3A4 in the resting form, (b) CYP3A4−metyrapone complex, (c) CYP3A4−progesterone complex in the peripheral binding site, and (d) CYP3A4−progesterone complex in the active site.

$RMSD_{init}$ values of CYP3A4 remain within 2.5 Å for 1.8 ns of simulation time. This indicates that the conformation of CYP3A4 is maintained stable irrespective of ligand binding, which is consistent with the stability of the overall protein structure toward ligand binding as revealed by X-ray crystallographic data.[28] It is interesting to note that, for bound simulations, the $RMSD_{init}$ values of ligands are lower than those of CYP3A4 C_α atoms during the entire course of the simulation.

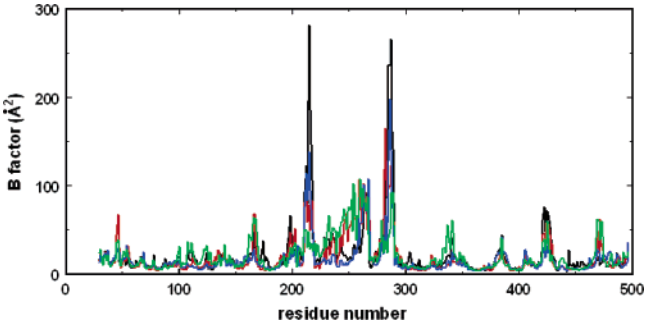

Figure 5. Calculated B-factors of the C_α atoms for ligand-free CYP3A4 (black), CYP3A4−metyrapone complex (red), CYP3A4−progesterone complex in the peripheral binding site (blue), and CYP3A4−progesterone complex in the active site (green).

Therefore, the movement of the ligands seems to be insignificant when compared to the conformational change of the protein, which is not surprising for a small size of the two binding sites.

To examine the change in dynamic flexibilities of the different regions of protein structure due to ligand binding, B-factors for the C_α atoms (B_i) of unliganded and liganded CYP3A4 were calculated using the following relationship:

$$B_i = \frac{8}{3}\pi^2\langle \Delta r_i \rangle^2 \qquad (2)$$

where $\langle \Delta r_i \rangle$ is the rms atomic fluctuation of the C_α atom of residue *i*. As shown in Figure 5, the overall B_i values of unliganded CYP3A4 are similar to those of the liganded ones, implying that the ligand binding has little effect on the flexibility of protein conformation in solution. However, we note that several residues show a significant change in B_i values in the presence of the inhibitor metyrapone and the substrate progesterone. The B_i values for the unliganded and the liganded CYP3A4 show a major peak in the region of residues 282−289, which is consistent with the absence of electron density at those residues in the X-ray crystal structures. A major peak is also observed for the ligand-free CYP3A4 in the region of residues 214−216 that are the components of the loop connecting F and F′ helices around the active site (Figure 3). Considering the proximity of the flexible loop to a channel running from bulk solvent to the active site, it can be argued that the high-amplitude motion of the flexible loop should be responsible for the broad substrate specificity of CYP3A4. However, binding of the inhibitor metyrapone and the substrate progesterone in the active site reduces the B_i value for Phe215 by 204.0 and 245.0 Å^2, respectively, suggesting that the motions of the highly flexible residues are restricted by binding of the ligands in the active site. The binding of progesterone in the peripheral binding site also seems to have an effect of lowering the motional amplitude of the flexible loop, which can be inferred from of the decrease in the calculated B_i values for Phe215 by 142.8 Å^2.

Structural Features of Unliganded and Liganded CYP3A4 in Solution. In the previous X-ray crystal structures of CYP3A4, no ordered water molecule was found in the active site, although it is expected that a low-spin ferric heme iron should have an additional axial ligand at the sixth coordination position.[28] In the present solution-phase MD simulation, however, a structural water molecule (Wat8217) that comes from bulk solvent is coordinated to the heme iron along a line perpendicular to the heme plane. As shown in Figure 6, the backbone aminocarbonyl group of Ala305 and an additional solvent molecule form a hydrogen bond with the structural water molecule, playing a role in positioning the axial water ligand around the heme iron in the active site. In contrast to the structural stability of the hydrogen bond between Wat8217 and Ala305, a rapid exchange is observed for the solvent molecule that acts as a hydrogen bond acceptor with respect to the structural water molecule. This indicates that complex solvent dynamics would be involved in maintaining the coordination geometry of the heme iron, which may be an explanation for the necessity of the channel connecting the active site and bulk solvent in the structure of CYP3A4.

Displayed in Figure 7 are the time evolutions of the internuclear distances associated with the interactions of the structural water molecule with the heme iron and with Ala305. It is noted that the distance between the water ligand and the heme iron remains around 2 Å during the entire course of simulation with the time average of 1.96 Å. Judging from such a dynamic stability, we determined that the coordination structure of the heme iron is stabilized by the ligation of a structural water molecule, which is also believed to participate in the catalytic mechanism of CYP3A4. Related to the role of a water molecule in the enzymatic reaction, it was proposed that a water ligand would be involved in the spin-state conversion of the heme iron and in the proton-transfer cascade that leads to heterolytic bond scission of oxygen.[62]

As can be seen in Figure 7, the hydrogen bond established between the backbone aminocarbonyl oxygen of Ala305 and the water ligand also exhibits a dynamic stability: it is maintained for 90% of simulation time, if the distance limit for the O···H hydrogen bond is assumed to be 2.2 Å as suggested by Jeffrey.[63] This result confirms the role of Ala305 in stabilizing the water ligand at the sixth coordination position of the heme iron. Indeed, the significant role of Ala305 in structure and function of CYP3A4 was well-attested in mutagenesis studies, which showed that the replacement of the amino acid residue at position 305 led to impaired catalytic activity.[64,65] Despite the overall dynamic stability of the hydrogen bond, we see that the two hydrogen atoms of the water ligand exchange their respective spatial positions to interact with the aminocarbonyl oxygen of Ala305 and another solvent molecule in an alternative manner. This is related to the dynamic replacement of the second water molecule that forms a hydrogen bond with the axial water ligand, further supporting the involvement of complex solvent dynamics in stabilizing the coordination geometry of the heme iron in the active site.

Figure 8 shows a representative MD trajectory snapshot of CYP3A4 complexed with metyrapone in solution. As in the X-ray crystal structure, one pyrimidinyl nitrogen (N14 in Figure 1) is coordinated to the heme iron as the sixth ligand, while the other (N1) is directed toward the side chain of Arg105. The pyrimidinyl ring and two methyl groups of the inhibitor form a stable van der Waals contact with the side chains of Ile301,

(62) Haines, D. C.; Tomchick, D. R.; Machius, M.; Peterson, J. *Biochemistry* **2001**, *40*, 13456−13465.
(63) Jeffrey, G. A. *An Introduction to Hydrogen Bonding*; Oxford University Press: Oxford, 1997.
(64) Domanski, T. L.; He, Y.-A.; Khan, K. K.; Roussel, F.; Wang, Q.; Halpert, J. R. *Biochemistry* **2001**, *40*, 10150−10160.
(65) Fowler, S. M.; Riley, R. J.; Pritchard, M. P.; Sutcliffe, M. J.; Friedberg, T.; Wolf, C. R. *Biochemistry* **2000**, *39*, 4406−4414.

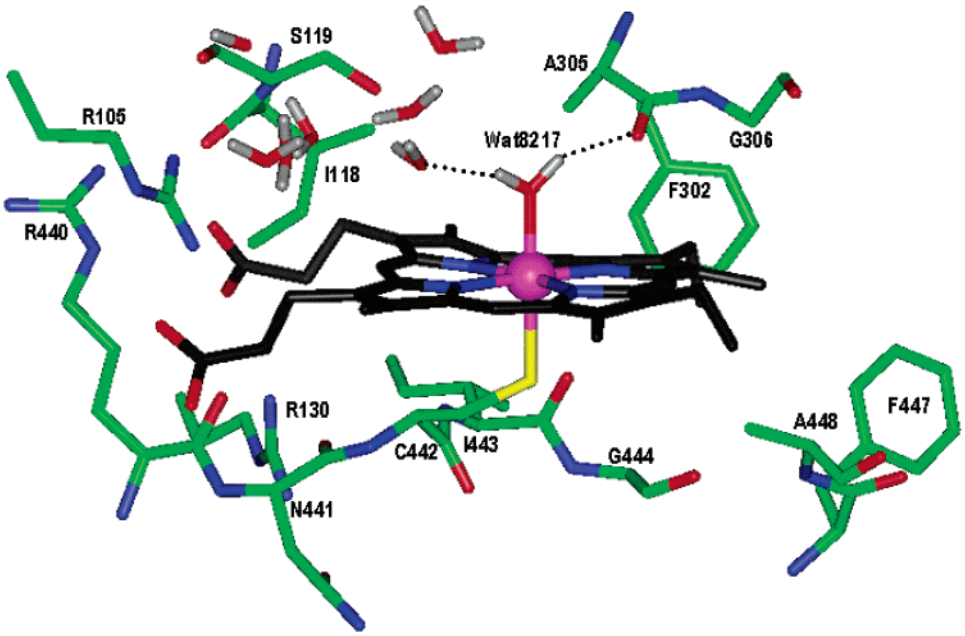

Figure 6. Representative MD trajectory snapshot of CYP3A4 in the resting form, including the solvent molecules found near the active site. The heme iron is represented by a pink ball. Each dotted line indicates a hydrogen bond.

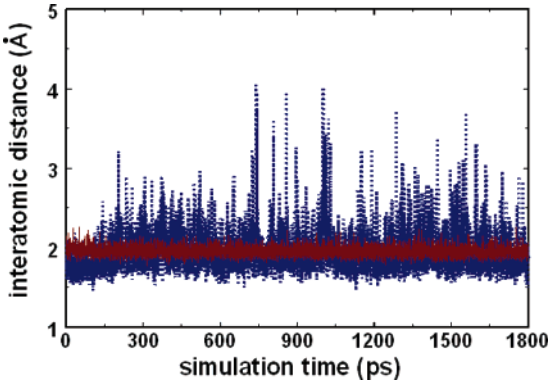

Figure 7. Time evolutions of the internuclear distances associated with water ligation to the heme iron (red) and the hydrogen bond between the water ligand and the backbone of Ala305 (blue).

Phe304, Ala305, Thr309, and heme, which has an effect of maintaining the ligation of N14 to the heme iron. Despite the residence of the inhibitor at the sixth coordination position, a few solvent molecules are also found around the heme iron to interact with the hydrophilic groups in the active site. This is a structural feature inconsistent with the X-ray crystal structure of the CYP3A4−metyrapone complex, in which no water molecules were found within the distance of 10 Å from the heme iron, although the inhibitor occupies a small portion of the active site volume and leaves sufficient space for additional molecules to get into the active site. Such a discrepancy can be attributed to the fact that the access of water molecules to the active site may depend on the crystallization procedure. It can also be argued that, as already indicated by Williams et al., the analysis of electron density at the active site was not accurate enough to detect all water molecules in the asymmetric unit. The solution-phase structure found in this MD study also differs from the crystal structure in that the inhibitor carbonyl group forms a hydrogen bond with the side chain of Ser119. This newly observed hydrogen bond can be related with the high inhibitory activity of metyrapone against the CYP enzymes.[66]

As an estimation of dynamic stabilities for the coordination of metyrapone to the heme iron and for the hydrogen bond between the inhibitor and Ser119, we have calculated time evolutions of the associated interatomic distances, and the results are plotted in Figure 9. It is noted that the distance between the heme iron and N14 falls under 2.5 Å for 92% of simulation time with the time average of 2.32 Å, comparing well with the coordination distance of 2.27 Å in the crystal structure. In the initial stage of simulation, the hydroxyl moiety of Ser119 resides at a distance of ∼5 Å from the inhibitor carbonyl group as in the crystal structure. However, a stable hydrogen bond is formed between the two groups after 10 ps of simulation time and maintained stable during the entire course of the simulation. Judging from the observed dynamic stabilities, a direct coordination to the heme iron and the formation of a hydrogen bond with Ser119 seem to be the significant binding forces that stabilize the CYP3A4−metyrapone complex in aqueous solution.

Figure 10 shows a representative MD trajectory snapshot for progesterone bound in the active site of CYP3A4. One carbonyl oxygen (O20) of progesterone forms a hydrogen bond with the side chain hydroxyl group of Ser119, while the other (O3) points toward the backbone aminocarbonyl group of Arg106. The terminal methyl group of progesterone is stabilized through hydrophobic interactions with the side chains of Phe304 and Ala305, further supporting a role of the latter in the oxidative degradation of progesterone by CYP3A4.[64,65] The steroid backbone of progesterone forms a stable van der Waals contact with the side chains of Arg105, Phe108, Phe215, and heme, with its five-membered ring being directed to the dioxygen molecule coordinated to the heme iron. The side chain of Ala370 resides in the vicinity of the steroid backbone at a distance of 4−5 Å, also playing a role in the stabilization of progesterone in the active site of CYP3A4. This is a structural feature consistent with the previous mutagenesis study, in which a mutation at residue 370 led to a substantial decrease in the rate

(66) Rossi, M. *J. Med. Chem.* **1983**, *26*, 1246−1252.

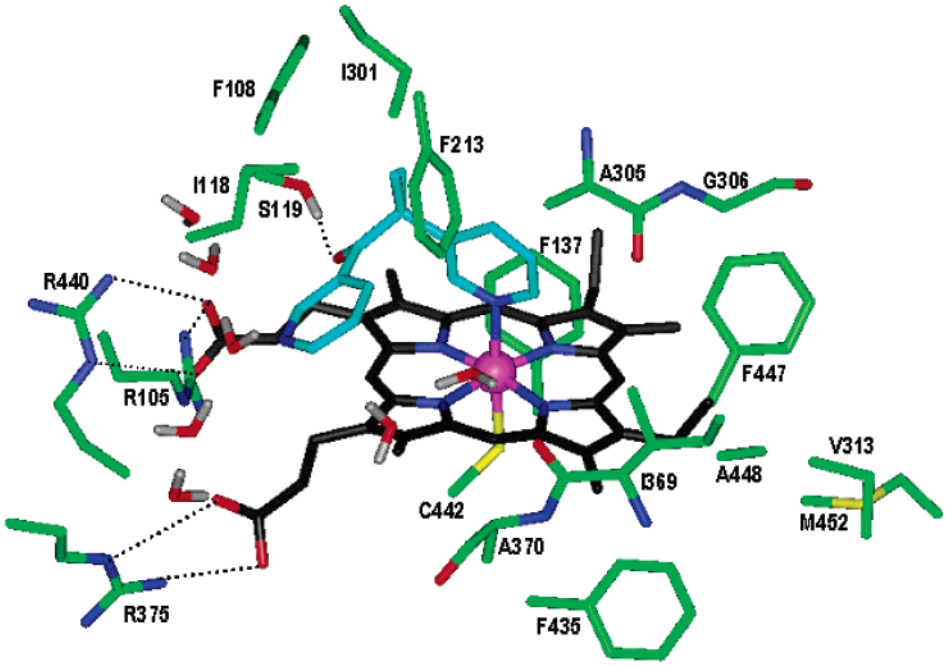

Figure 8. Representative MD trajectory snapshot for the CYP3A4−metyrapone complex, including the solvent molecules found near the active site. Carbon atoms of active site residues, heme, and metyrapone are indicated in green, black, and cyan, respectively. Each dotted line indicates a hydrogen bond.

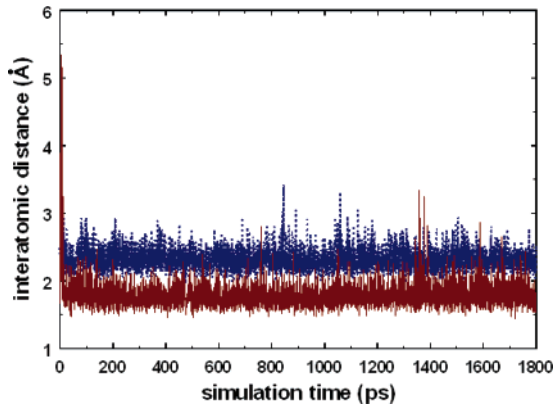

Figure 9. Time evolutions of the interatomic distances associated with the ligation of metyrapone to the heme iron (blue) and the hydrogen bonding of metyrapone with Ser119 (red).

of CYP3A4-catalyzed hydroxylation of progesterone.[20] In contrast to the CYP3A4−metyrapone complex, no water molecules are found around the heme iron in the active site, which is not surprising for the increased molecular size and hydrophobicity of progesterone as compared to that of metyrapone and the presence of dioxygen at the sixth coordination position. However, a hydrogen bond network of several solvent molecules resides in the proximity of the substrate at the entrance of the active site, supporting the possibility that water molecules would be involved in the catalytic reaction. In this regard, it was proposed that the ordered water molecules around the active site should act as proton donors in the oxidative degradation of the substrates by CYPs.[60]

Figure 11 shows time dependences of the internuclear distances associated with the interactions of progesterone in the active site of CYP3A4. It is noted that the distance between one carbonyl oxygen of progesterone (O20) and the side chain hydroxyl group of Ser119 remains within 2.2 Å during the entire course of the simulation. Judging from such a dynamic stability of the hydrogen bonds observed in both CYP3A3−metyrapone and CYP3A4−progesterone complexes, we observe that the formation of a stable hydrogen bond with Ser119 seems to be a significant binding force that stabilizes the inhibitor and the substrate in the active site of CYP3A4. Related with the catalytic mechanism for the oxidative degradation of progesterone by CYP3A4, it was proposed that the activated oxygen in the active site abstracts hydrogen atoms at the C6 and C16 positions,[20] leading to the formation of the final hydroxylated major metabolite. In the structure of the CYP3A4−progesterone complex in aqueous solution, we note that the C16 atom of progesterone resides in the vicinity of the dioxygen molecule coordinated to the heme iron. The associated interatomic distance between C16 and the O1 atom of dioxygen is maintained within 3−5 Å for 68% of the simulation time. Thus, the structural and dynamic features of the CYP3A4−progesterone complex found in this solution-phase MD simulation studies support the catalytic mechanism involving the hydroxylation at the C16 position. In order for the mechanism involving the oxidation at the C6 position to be supported, we should be able to find a CYP3A4−progesterone complex in which the O3 end of the substrate resides near the heme iron in the calculations. Despite an extensive search of docking solutions and MD trajectories, however, such a configuration is not observed. Considering the fact that CYP3A4 may exist in multiple conformations both in solutions and in microsomal membranes,[67] we believe that a binding mode of progesterone supporting the hydroxylation at C6 could be found if the simulations are carried out at much longer time scales than our current computing power allows. Another possibility is that a conformationally different X-ray structure of CYP3A4 might be available in the future, from which the mechanism involving the hydroxylation at C6 could be supported.

(67) Davydov, D. R.; Halpert, J. R.; Renaud, J. P.; Hui Bon Hoa, G. *Biochem. Biophys. Res. Commun.* **2003**, *312*, 121−130.

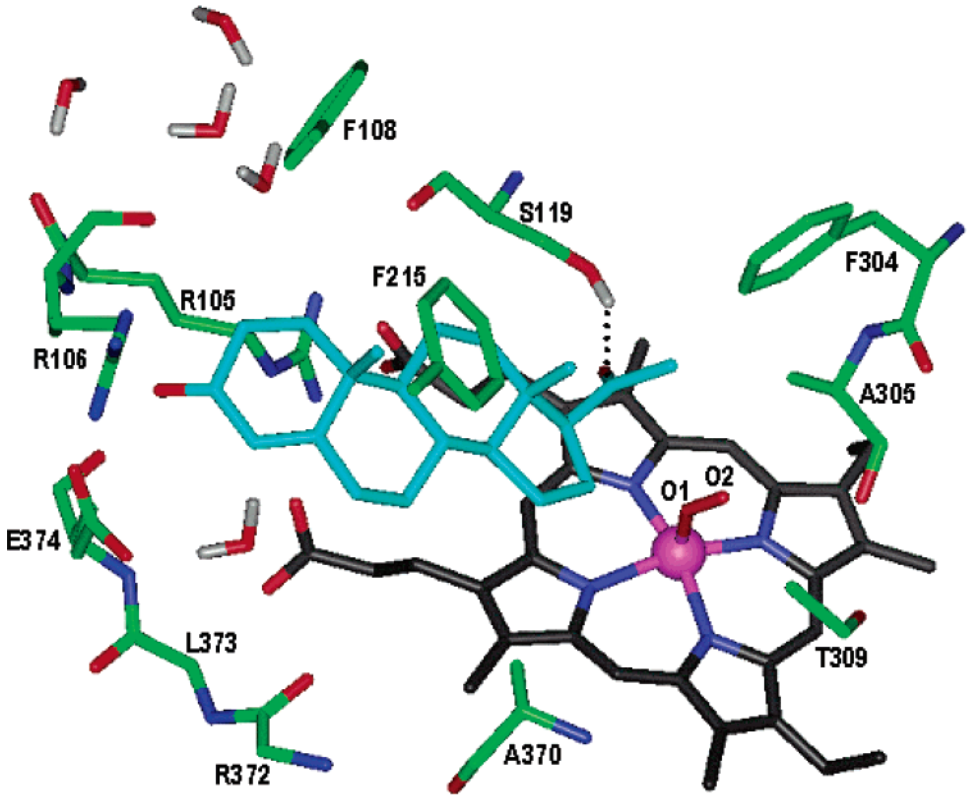

Figure 10. Representative MD trajectory snapshot for the CYP3A4−progesterone complex, including the solvent molecules found near the active site. Carbon atoms of active site residues, heme, and progesterone are indicated in green, black, and cyan, respectively. The dotted line indicates a hydrogen bond.

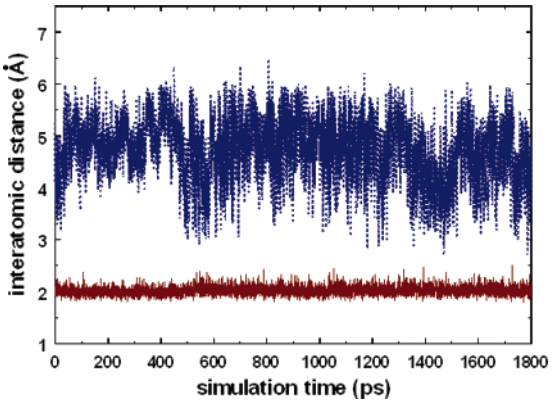

Figure 11. Time evolutions of the interatomic distances between HG atom of Ser119 and O20 atom of progesterone (red), and between O1 atom of dioxygen and C16 atom of progesterone (blue). See Figures 1 and 10 for identification of the atoms.

Conclusions

We have investigated the structural and dynamic properties of ligand-free CYP3A4 and its complexes with the substrate progesterone and the inhibitor metyrapone based on molecular dynamics simulations with the newly developed force field parameters for the heme−thiolate group and its dioxygen adduct. The calculated dynamic properties indicate that the malleability of the loop containing the residues 214−216 should be responsible for the broad substrate specificity of CYP3A4. The high-amplitude motion of the flexible loop is found to be damped out in the presence of the inhibitor and the substrate in the active site. A characteristic feature that discriminates the structure of the active site in solution from that in the X-ray crystal structure is the presence of a structural water molecule from bulk solvent at the sixth coordination position of the heme iron, forming a stable octahedral coordination geometry. A significant dynamic stability is observed for the direct coordination of the structural water molecule and metyrapone to the heme iron. A hydrogen bond between the side chain of Ser119 and a carbonyl group is found to be a significant binding force that stabilizes both the inhibitor and the substrate in the active site of CYP3A4. The structural and dynamic features of the CYP3A4−progesterone complex are consistent with the mechanism for the oxidative degradation of progesterone involving the hydroxylation at the C16 position by the reactive oxygen coordinated to the heme iron.

Acknowledgment. This work was supported by Grant No. R01-2004-000-10354-0 from the Basic Research Program of the Korea Science & Engineering Foundation. The authors would also like to acknowledge the support from KISTI (Korea Institute of Science and Technology Information) under "The Sixth Strategic Supercomputing Support Program" with Dr. Sang Min Lee as the technical supporter. The use of the computing system of the Supercomputing Center is greatly appreciated.

Supporting Information Available: The full author lists of refs 23 and 55. This material is available free of charge via the Internet at http://pubs.asc.org.

JA053809Q